

DISCUS - The Deep Interior Scanning CubeSat mission to a rubble pile near-Earth asteroid

Patrick Bambach^{1*} Jakob Deller¹ Esa Vilenius¹ Sampsa Pursiainen² Mika Takala² Hans Martin Braun³
Harald Lentz³ Manfred Wittig⁴

1 Max Planck Institute for Solar System Research, Justus-von-Liebig-Weg 3, 37077 Göttingen, Germany

2 Tampere University of Technology, PO Box 527, FI-33101 Tampere, Finland

3 RST Radar Systemtechnik AG, Ebenaustrasse 8, 9413 Oberegg, Switzerland

4 MEW-Aerospace UG, Hameln, Germany

* bambach@mps.mpg.de

Submitted to Advances in Space Research

Abstract

We have performed an initial stage conceptual design study for the *Deep Interior Scanning CubeSat* (DISCUS), a tandem 6U CubeSat carrying a bistatic radar as the main payload. DISCUS will be operated either as an independent mission or accompanying a larger one. It is designed to determine the internal macroporosity of a 260–600 m diameter Near Earth Asteroid (NEA) from a few kilometers distance. The main goal will be to achieve a global penetration with a low-frequency signal as well as to analyze the scattering strength for various different penetration depths and measurement positions. Moreover, the measurements will be inverted through a computed radar tomography (CRT) approach. The scientific data provided by DISCUS would bring more knowledge of the internal configuration of rubble pile asteroids and their collisional evolution in the Solar System. It would also advance the design of future asteroid deflection concepts. We aim at a single-unit (1U) radar design equipped with a half-wavelength dipole antenna. The radar will utilize a stepped-frequency modulation technique the baseline of which was developed for ESA’s technology projects GINGER and PIRA. The radar measurements will be used for CRT and shape reconstruction. The CubeSat will also be equipped with an optical camera system and laser altimeter to support navigation and shape reconstruction. We provide the details of the measurement methods to be applied along with the requirements derived of the known characteristics of rubble pile asteroids. Additionally, an initial design study of the platform and targets accessible within 20 lunar distances is presented.

Keywords:

Deep-space CubeSat, near earth asteroids, rubble pile asteroid, radar, computed radar tomography

1 Introduction

The goal of this paper is to advance the mission design for recovering the deep interior structure of an asteroid using small spacecraft. We introduce the

initial stage mission concept, the *Deep Interior Scanning CubeSat* (DISCUS), in which the goal is to fly two identical six-unit (6U) CubeSats ([Figure 1](#)) as a tandem into the orbit of a small rubble pile asteroid and to resolve its global interior structure via

tomographic radar measurements. This is an important scientific objective which has been approached via several mission concepts (Safaenili et al., 2002; Asphaug et al., 2003; Herique and Ciarletti, 2016; Kofman et al., 2007; Snodgrass et al., 2017). In particular, we approach the *Deep Interior* concept by Asphaug et al. (2003) as a state-of-the-art small spacecraft mission (NASA Mission Design Division, 2015) which can be either independent or accompanying a larger one. DISCUS CubeSats will be equipped with a bistatic penetrating radar and an optical imaging system. The design is derived from airborne Ground Penetrating Radar (GPR) which is today applied in mapping subsurface glacier and soil structures, e.g., ice thickness (Rutishauser et al., 2016; Gundelach et al., 2010; Eisenburger et al., 2008; Fu et al., 2014).

The first realized tomography attempt for small a Solar System body was the COMET Nucleus Sounding Experiment by Radio-wave Transmission (CONSERT) (Kofman et al., 2007, 2015) during the European Space Agency's (ESA) *Rosetta* mission in 2014. In CONSERT, a radio-frequency signal was transmitted between the *Rosetta* orbiter and its lander *Philae*. *Rosetta* was a major scale mission with its total budget of 1.4 Billion Euro with the cost of the lander being 200 Million. Even though the missions have been a success the high costs hinder the development of a comparable successor on this scale. Due to lower cost and the recent technological advances, small spacecraft would enable the exploration of both asteroids and comets more flexibly and in higher numbers. For comparison, the recently published M-ARGO concept aims for a budget of 25 Million Euro (Walker et al., 2017). The interest towards using CubeSats to complement traditional planetary missions is constantly increasing and, therefore, mission design to support this development is needed. A few years ago, Staehle et al. (2013) published an initial report on potential Interplanetary CubeSats with 2U science payload and 2U propulsion module. Later on in 2014, NASA announced with NeaScout the first detailed mission design of a 6U CubeSat to fly with a solar sail to an asteroid (Frick et al., 2014). Recently developed CubeSats capable of operating in deep space include the Lunar IceCube (Clark et al., 2016) and Mars Cube One (Asmar and Matousek,

2014; Rahmat-Samii et al., 2017; Hodges et al., 2016).

In Imken et al. (2017), the current status of 6U Interplanetary CubeSat development at the Jet Propulsion Laboratory (JPL) is given. Critical hardware, such as data handling and communication systems have been developed as standard buses at JPL. Namely, the Sphinx data handling system and the Iris transponder. The volume and weight of this hardware show that the promise of 6U interplanetary CubeSats with around 2U housekeeping, 2U propulsion and almost 2U payload could be kept. An ESA/ESTEC study found the limitations of 6U for a NEA mission to be critical, especially regarding on thermal management and Δv requirements of independent interplanetary missions. Therefore, a 12U based CubeSat concept M-ARGO (Walker et al., 2017) has been investigated and found promising. Besides completely autonomous missions also so-called CubeSat piggy-bag missions can become more common in the future. In the piggy-bag approach, a mothership transports the CubeSats to its target, deploys them and serves as a communication link. The advantage is that the requirements for navigation, communication, propulsion and total ionizing dose (TID) are reduced. For example, the plans of the unrealized Asteroid Impact Mission (AIM) included two CubeSats and the Mascot-2 lander (Michel et al., 2016; Herique and Ciarletti, 2016).

DISCUS (Figure 1) is designed to detect the internal macroporosity of an Itokawa-size (Abe et al., 2006) 260 to 600 m diameter *Near Earth Asteroid* (NEA) from a few kilometers distance. The primary goal of DISCUS will be to achieve a global signal penetration as well as to analyze the scattering strength for various different penetration depths and measurement positions. Additionally, forming an actual 3D reconstruction based on the measurements will be attempted. Using the reflected wave, also the shape of the body can be determined. Due to the many limitations of space missions, e.g., the strict payload and energy bounds, our radar design aims at a minimal weight and power consumption. Akin to airborne GPR, we apply the stepped-frequency measurement technique and a half-wavelength dipole antenna (Fu et al., 2014). Maximizing the detectability of deep structures such as voids necessitates using a signal

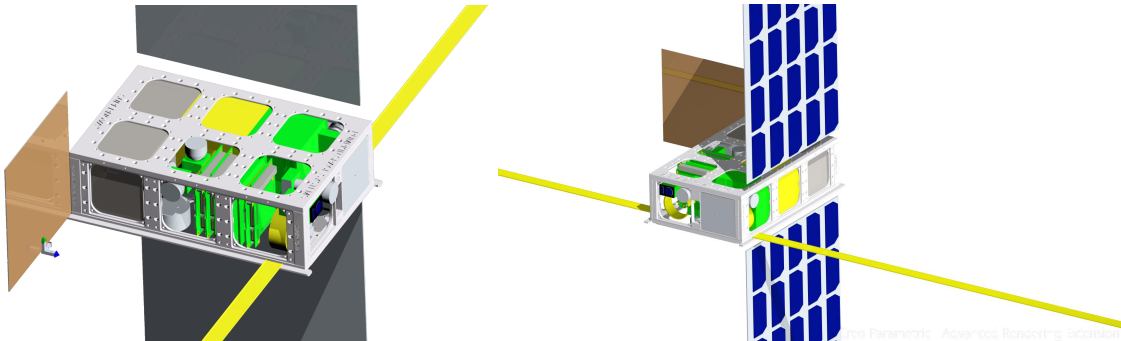


Figure 1: Conceptual pictures of the 6U DISCUS design containing (a) 1U radar (green), (b) 1U Communication (yellow), (c) 2U BIT-3 propulsion system (gray). Attached to the frame is a linear half-wavelength dipole antenna (yellow line). During the launch, the antenna will be rolled up. The other parts are components of the shelf (COTS). Among others a Pumpkin 6U frame with four star trackers, an altimeter, a camera, three reaction wheels and PCB boards for housekeeping and a cold gas thruster. Two solar panels are oriented in a perpendicular direction with respect to the antenna. The radar measurement is performed with the antenna pointed towards the sun in order to minimize the noise caused by solar radiation. It also maximizes the power gain of the solar panels and reduces the need for power storage.

frequency below 100 MHz (Francke and Utsi, 2009; Leucci, 2008; Kofman, 2012). We initially target at 20–50 MHz center frequency in the radar design.

This paper is structured as follows. In Section 2, we motivate the mission plan via a brief review of what is known of rubble pile asteroids. Section 3 describes the on-board scientific instruments and their use. We provide the details of the measurement methods to be applied along with the requirements derived from the known characteristics of the rubble pile asteroids. Section 4 sketches the mission layout. An initial design concept of the platform and accessible targets is presented. Section 5 is devoted to the discussion. Finally, Section 6 concludes the paper and summarizes the study.

2 Rubble pile asteroids in the Solar System

When the Solar System was formed 4.6 Ga ago, planetesimals constituted the building blocks of protoplanets and eventually the planets themselves. Comets and asteroids are the remainders of this early

stage. Exploring their population is a key to understanding the Solar System’s history and evolution, although they contain only about 0.002 % of its total mass. The asteroids have evolved through several processes; space weathering changed their surface by effects of radiation, internal heating may have altered their chemistry and mineralogy, and collisional events transformed their interior structure and size distribution. According to the present knowledge, most of the asteroids are actually resulting from catastrophic disruptions of large parent bodies (Farinella et al., 1982). Namely, modeling of catastrophic disruptions (Michel et al., 2001, 2002) can reproduce the size distribution of the Karin asteroid family, showing that many fragments re-accumulated to form rubble pile asteroids.

The current evidence also shows that these processes have left most of the asteroids in the size range of about 200 m to 100 km with an interior that is not monolithic but rather an agglomerate of smaller fragments, bound together mainly by gravity and only weak cohesion (Richardson et al., 2002).

The rough comparisons between the meteoritic materials and the indirect density estimates suggest

that many asteroids have a large amount of internal macroporosity, that is, voids larger than the typically micrometer sized cracks in the matrix of meteoritic samples (denoted as microporosity). Recently, Carry (2012) found high percentages of macroporosity by comparing mass and volume of 287 asteroids, and aggregating information about meteoritic samples linked to their taxonomic classes. For example, the estimate $P_{\text{macro}} = 72 \pm 14 \%$ was obtained for asteroid (854) Frostia. The measurements provided by the recent Hayabusa and Rosetta missions have also shown that the small asteroid Itokawa (Figure 2a, Saito et al., 2006; Abe et al., 2006) as well as the larger one Šteins (Figure 2b) might have around 40% of macroporosity, respectively. Moreover, simulations of granular flowing material match well with the observed top-like shape of many observed asteroids, e.g., Šteins; simulating the spin-up of rotating asteroids, Walsh et al. (2008) as well as Sánchez and Scheeres (2012) found a material flow towards the equator, forming asteroids with comparable shapes. Analyzing the rotation period as a function of the size has revealed that, for asteroids larger than 200–300 m, there exists a general cut-off at a period of 2.2 hours which only some so-called superfast rotators such as the asteroid 1950 DA¹ surpass (Pravec et al., 2002; Rozitis et al., 2014). This spin barrier (e.g. Pravec and Harris, 2000; Kwiatkowski, 2010) is coinciding with the limit for a cohesionless body before it starts losing mass at the equator, which indicates that most bodies larger than 200–300 m in diameter are not monolithic in the interior.

While the evidence for a shattered interior of asteroids is strong, the exact configuration of the interior of these objects is unclear, as direct measurements are still missing. Macroporosity can arise from void space inside the asteroid at various different scales. There might be large void fractures at the scale of hundreds of meters in the interior, as shown to be likely for Šteins (Figure 2b, see details in Deller, 2017), or small scale cavities caused by interlocking of boulders. Moreover, the sorting effects of the granular mechanics suggest that the asteroid Itokawa might be a rubble pile with large constituent frag-

ments, explaining the enhancement of the large boulders on its surface. Namely, the amount of regolith observed on Itokawa’s surface is significantly larger than what could be produced by impact events forming the observed number of surface craters (Barnouin-Jha et al., 2008). Itokawa’s *rough highlands* terrain is covered with rubbles following a cumulative power law distribution of -3.1 ± 0.1 , and the number of large boulders is enhanced compared to models of re-aggregation after a catastrophic impact event, which most likely formed the asteroid (Michikami et al., 2008). Indirect inferences of the macroporosity structures can also be obtained through the simulation of the impact events which allows one to connect the crater structure to the surface features and also to determine the shock wave propagation characteristics inside the asteroid. Deller (2017) demonstrated this method on asteroid Šteins, showing that the catena of pits running from the rim of the crater on Šteins can be interpreted as a sequence of sinkholes into an interior crack, which has opened due to the impact.

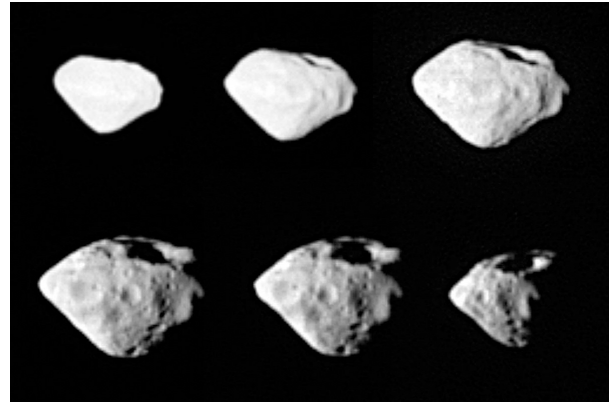
The mission proposed here provides the means to finally sample the interior of a rubble pile asteroid directly and to provide direct measurements about the distribution of porosity inside these objects. The knowledge obtained would be vital, for example, for the assessment of the asteroid impact deflection as a possible way to neutralize threats by potentially hazardous earth colliding asteroids. Namely, the internal structure is of crucial importance in this regard, since the scale of the porosity inside asteroids determines the propagation of shock waves and, therefore, the efficiency of energy transfer during impact events. Another important application would, obviously, be the mineralogy of asteroids, since the proposed radar measurement technique would provide first-hand information of the dielectric properties in the interior (Michel et al., 2015).

NEAs that are easy to reach for space missions have been explored, e.g., in the Mission Accessible Near-Earth Objects Survey (MANOS, Thirouin et al., 2016) focusing on NEAs that have orbital parameters with low Δv , i.e., low relative velocity with respect to the Earth. For a small, but well-described sample of 86 sub-kilometer sized asteroids, it rated seven of these objects as possible targets for manned

¹<https://cneos.jpl.nasa.gov/doc/1950da/>



(a) Image of the asteroid Itokawa taken by the Hayabusa spacecraft. Source: JAXA, http://global.jaxa.jp/article/special/hayabusa_sp3/index_e.html



(b) Asteroid Šteins imaged by the OSIRIS camera system on board of Rosetta. Source: ESA © 2008 MPS for OSIRIS Team MPS/UPD/LAM/IAA/RSSD/INTA/UPM/DASP/IDA

Figure 2: Itokawa and Šteins, two rubble pile asteroids visited by spacecraft.

missions. Using expectations on the number of NEAs from de-biasing studies of the NEA population (Tricarico, 2017), Thirouin et al. (2016) estimate that a total number of approximately 33 000 NEAs are accessible for space missions in the Thirouin et al. (2016) definition.

3 Scientific instrumentation

3.1 Stepped-frequency radar

The radar design of DISCUS is based on the stepped-frequency technique which requires a relatively low DC power and low data rate. This is possible since, instead of a single full-bandwidth signal pulse, narrow frequency bands are transmitted and received separately. As the stepped-frequency technique allows measurement of weaker bands, it is generally used in radars with a narrow instantaneous bandwidth as compared to the total bandwidth of the resolution aimed (Lacomme, 2001).

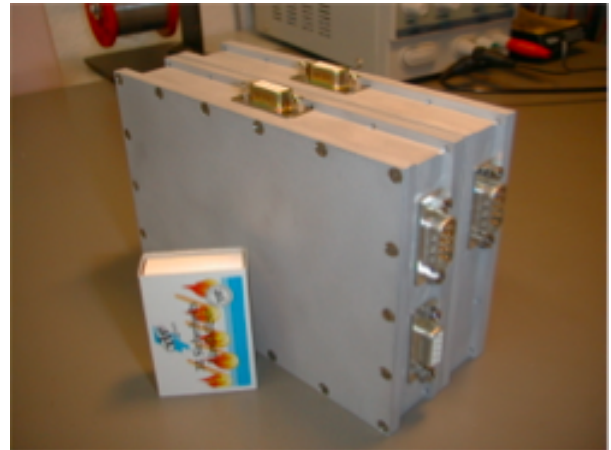


Figure 3: Stepped-frequency radar for the HOPE (Handheld Operated Demining System) (RST Radar Systemtechnik AG, 2001). The dimensions of the box are $12\text{ cm} \times 15\text{ cm} \times 5\text{ cm}$ and its volume is 900 cm^3 .

3.1.1 Mathematical concept

The set of transmitted narrow frequency lines $\psi_1, \psi_2, \dots, \psi_N$ allows one to approximate a given function f via the sum $f = \sum_{\ell=1}^N c_\ell \psi_\ell$. If φ_ℓ is the received signal (data) corresponding to frequency line ψ_ℓ , then the data g resulting from a transmission f is approximately given by $g = \sum_{\ell=1}^N c_\ell \varphi_\ell$, where the coefficients c_1, c_2, \dots, c_N follow from the formula for f . Hence, the data g for any transmission f within the given frequency range can be approximated, if the function pairs ψ_ℓ and φ_ℓ for $\ell = 1, 2, \dots, N$ are given, i.e., if the stepped-frequency measurement data are available. For a mathematical study of the DISCUS radar, please refer to [Takala et al. \(2017a\)](#).

3.1.2 Baseline design

The stepped-frequency radar design referred to in this study was originally developed and verified by *RST Radar Systemtechnik AG* within the European Space Agency’s (ESA’s) GINGER (Guidance and Into-the-Ground Exploration Radar) project ([Lentz and Braun, 2000](#); [Putz et al., 1997](#)), where a planetary rover was used as the reference platform. In a subsequent ESA project PIRA (Planetary Into-the-Ground Radar and Altimeter) this technology was verified under platform movement using a helicopter as the carrier ([Braun et al., 1997](#)). In addition to space systems, RST has also previous experience on packing a stepped-frequency radar into a very small volume. For example, in the HOPE (Handheld Operated Demining System) landmine detector the total radar volume was 900 cm^3 ([Figure 3](#)).

3.1.3 DISCUS radar

In the 6U DISCUS design, the goal is to fit a radar with a 2 MHz total signal bandwidth and 20–50 MHz center frequency into a 1U cube (1000 cm^3). The lower end of the targeted frequency interval is advantageous in order to achieve an appropriate signal penetration ([Kofman, 2012](#)) and to minimize solar noise. Namely, if the Sun is active, the dominating error source will be the solar radiation (see [Figure 4](#)) which is on a comparably low level at the targeted interval decreasing towards the lower frequen-

cies ([Kraus, 1966](#)). The minimum total effect of the active Sun and the galactic background corresponds to about 20 ± 5 MHz, since the galactic noise increases towards the low frequencies. In order to minimize the effect of the Sun, the antenna will be pointed towards it during the measurement. The targeted radar specifications have been listed in [Table 1](#).

The duration of a single frequency line can be estimated via $\tau = 1/B_\ell$, where $B_\ell = B/N$, i.e., the total bandwidth B is divided by the number N of the frequency lines, roughly around 64 lines with pulse duration $32 \mu\text{s}$ can be transmitted and received separately from a 5 km distance to the asteroid (the pulse duration is 96% of the total travel-time). A sufficient pulse repetition time (PRT) with respect to the corresponding decay time will be $150 \mu\text{s}$, i.e., the duration of the complete pulse sequence will be about 9.6 ms at the 5 km distance. The narrower is B_ℓ the longer is the single pulse duration and the more energy is transmitted. Even when assuming at worst a ground speed of a few meters per second, a sufficient number frequency lines could be measured. Lower speed would hereby enable to transmit and receive more lines and enhance the signal-to-noise ratio. The stepped-frequency sequences for larger measurement ranges can also be longer in time and, thereby, contain more lines in order to extend the ambiguity and dynamic range. For each frequency band, the spectrum of the signal is recorded for a time interval determined by the observation distance.

3.1.4 Link budget and measurement noise

The initial link budget ([Table 2](#)) for the received signal is here approximated in decibels via the equation $P_{RX} = P_{TX} + G_{TX} + S + G_{RX}$ where $P_{TX} = 0$ dB (10 W) and P_{RX} denote the transmitted and received power, S the signal power at the receiver location based on an isotropic radiator model, with an isotropic source and effective antenna aperture $A_{eff} = \lambda^2/(4\pi)$, and G_{TX} and G_{RX} the gain of the transmitting and receiving half-wavelength dipole antenna, that is, ($G_{TX} = G_{RX} = 2.15$ dBi).

In order to obtain an estimate for S_R , we simulated the planned radar measurement numerically ([Takala et al., 2017a](#)) using a 550 m diameter syn-

Table 1: Targeted radar parameters.

• Center frequency:	20–50 MHz
• Antenna length:	Two times 1.5–3.75 m ($\lambda/2$)
• Radar modulation:	32 to 2048 lines
• Pulse duration (5 km distance):	32 μ s
• Pulse repetition time (5 km distance):	150 μ s
• Input/ Transmitting power:	40 W/ 10 W
• Receiver bandwidth:	2 MHz
• Size:	1 U
• Weight:	1 kg

thetic asteroid model based on the surface shape of 1998 KY26² (Figure 4). The center frequency of the measurement was assumed to be 20 MHz, the measurement distance 5 km and the number of frequency lines $N = 64$. The relative dielectric permittivity distribution ε_r enclosed by the surface consisted of a background part ($\varepsilon_r = 4$), a 40 m thick surface layer ($\varepsilon_r = 4$) and three 60 to 100 m diameter voids ($\varepsilon_r = 1$) located in the deep interior part. The average signal attenuation rate was around 25 dB/km corresponding to a porous basalt at the chosen frequency (Kofman, 2012). The peak power P_{RX} received for the surface layer and a void in the depth of 150 m was -120 dB and -128 dB, respectively.

The relative measurement noise levels (Table 2) caused by the spectral radiation flux density F (Kraus, 1966) from the active and quiet Sun (2E-19 and 2E-23 W/m²/Hz) as well as from the galactic background (5E-20 W/m²/Hz) were estimated via the formula $10 \log_{10}(FB_{\ell}A_{eff}/P_{TX})$ in which $A_{eff} = 0.13\lambda^2$ is the effective aperture of the half-wavelength dipole antenna, B_{ℓ} the bandwidth of a single frequency line, and P_{TX} is expressed in Watts, respectively. Our experience is that the data can be inverted when the total measurement noise level is at least 5–10 dB below the peak level of P_{RX} (Takala et al., 2017a,c). In (Jol, 2008; Erst, 1984), -8 dB has been suggested as the maximal tolerable noise level for penetrating radar measurement. That is, losses related to penetration, hardware, and signal processing, and miscellaneous reasons can at 5 km

distance amount to a total of roughly around 7–15 dB using the galactic background noise as a reference. Due to the two-way signal path and the linear distance dependence of the (stepped-frequency) pulse length, approaching the asteroid from the distance d_0 to d_1 would increase P_{RX} in decibels approximately according to the formula $\Delta_{P_{RX}} \approx 30 \log_{10}(d_0/d_1)$ which gives $\Delta_{P_{RX}} \approx +5$ dB for $d_1 = 3.5$ km and $\Delta_{P_{RX}} \approx +9$ dB for $d_1 = 2.5$ km.

3.1.5 Computed radar tomography

Tomographic analysis of the targeted NEA can be performed akin to ordinary tomographic GPR surveys in which radio frequency signals enable reconstructing subsurface ground layers. Based on the radar specifications, the range resolution ($\delta_r = c/(2B)$ with c denoting the signal velocity and B the bandwidth) determining the minimum distance between two separable details is 20 to 40 m inside the NEA, assuming that its relative electric permittivity is 3 to 12 (e.g. solid and pulverized rocks and silica). On ground, the numerical simulations necessary for inverting the radar measurements can be performed using a state-of-the-art computer or computing cluster with sufficient memory for running iterative wave equation solvers within a three-dimensional computation domain. Our recent simulation study demonstrates that a 2 MHz full-wave (full-bandwidth) data can be computed and inverted for the targeted asteroid size range using a high-end workstation computer equipped with up-to-date graphics processing units (GPUs) (Takala et al., 2017a).

²<https://ssd.jpl.nasa.gov/sbdb.cgi?sstr=1998KY26>

Table 2: Initial data link budget and noise level estimates for 5 km orbiting distance, 20 MHz center frequency, 2 MHz bandwidth, and 10 W transmission power.

• Transmitted power P_{TX}	0 dB
• Half-wavelength dipole antenna gain $G_{TX} = G_{RX}$	2.15 dBi
• Peak power P_{RX} received for the surface layer	-120 dB
• Peak power P_{RX} received for a void at 150 m depth	-128 dB
• Measurement noise due to active Sun	-137 dB
• Measurement noise due to quiet Sun	-177 dB
• Measurement noise due to the galactic background	-143 dB

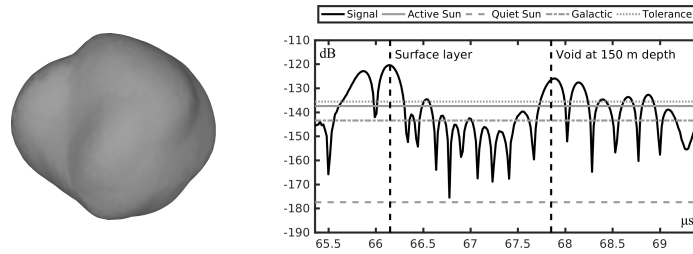


Figure 4: **Left:** The surface model of the asteroid 1998 KY26 scaled to a diameter of 550 m to examine the relative received power P_{RX} for a 10 W signal pulse with 20 MHz center frequency and 2 MHz bandwidth (Takala et al., 2017a). **Right:** The backscattered signal power P_{RX} (dB) received by the transmitting spacecraft at 5 km orbiting distance to the asteroid. The peaks reflecting from a surface layer and a void at 150 m depth have been marked with vertical lines. The noise levels corresponding to active and quiet Sun and the galactic background have been illustrated with horizontal lines. Also, the maximal theoretical noise tolerance -8 dB suggested for a penetrating radar signal (Jol, 2008; Erst, 1984) is shown. The x -axis shows the propagation time of the signal (μ s).

To record the tomography data, we will use a simple bistatic (two-spacecraft) measurement scenario in which the CubeSats will be placed within a (nearly) constant angle γ from each other as seen from the NEA. One of the CubeSats will both transmit and receive the signal and the other one will serve as an additional receiver. As the instrumentation on both CubeSats is identical the concept is redundant by its design. The reference phase can be transmitted by the master satellite. The flying formation does not necessarily need to be maintained stationary: the mutual distance between the CubeSats can slightly vary during the measurements, since their positions will be tracked independently. At least the following two different choices for γ will be used: (i) $\gamma \leq 35^\circ$ and (ii) $\gamma \geq 145^\circ$. The first one of these (i) will enable an enhanced backscattering measurement; our numerical results (Takala et al., 2017a) suggest that with the choice $\gamma = 25^\circ$ the accuracy and reliability of the bistatic tomography outcome is superior compared to the monostatic (single-spacecraft) case. The second option (ii) will allow a higher signal-to-noise ratio due to one-way signal paths and tomographic travel-time measurements, performed, e.g., in CONSERT (Takala et al., 2017b; Kofman et al., 2015).

3.2 Shape model

The altimeter-based shape model of the asteroid can be reconstructed via a combined use of radar and laser measurements. The laser data will complement the radar measurements in which the first return coming from the surface of the asteroid is detected. Generally, the topographic (flat surface) height accuracy δ_{th} is below 20% of the range resolution (Manasse, 1960). Consequently, in empty space, a measurement with the bandwidth of 2 MHz has the range resolution of $\delta_r = 75$ m and height accuracy of about $\delta_{th} = 15$ m. These values are independent of the operation distance. The latter one serves as a rough estimate for the shape model reconstruction accuracy assuming that a sufficiently dense distribution of points over the asteroid surface can be covered at the orbit.

3.3 Optical imaging

A visual camera system is needed to enhance the accuracy of spacecraft positioning. The images provided by the camera can also be used to optimize the shape model. Because of the limited data transmission rate and the resulting constraints on the data volume, the angular resolution of the camera has to be chosen to provide a surface coverage with a reasonable amount of images in the expected orbit. Without detailed analyses available at this point, we build our estimate on the experience from the Hayabusa mission (Ishiguro et al., 2010). The AMICA imaging system (Nakamura et al., 2001) on the Hayabusa spacecraft took a total of > 1400 images of asteroid Itokawa. The camera had a field-of-view (FOV) of $5.83^\circ \times 5.69^\circ$, and a detector with $1024 \text{ px} \times 1000 \text{ px}$. The analog-to-digital converter sampled the signal with 12 bit resolution. This corresponds to an image file size of 1.46 MiB uncompressed. Lossless compression can achieve an estimated factor 2 in file size reduction. Therefore, we expect to need to downlink a total of ≈ 1025 MiB over the course of the mission in order to achieve a shape model for a scenario similar to Hayabusa. Commercial of the shelf camera systems mounted on small satellite platforms achieve a FOV of about 15° . While the lower resolution directly decreases the resolution achievable for the surface shape model, the estimate of the data volume is still applicable.

4 Mission layout

4.1 Overall design

For the 6U design of DISCUS, mostly components of the shelf (COTS) have been selected. The spacecraft is illustrated in Figure 1. The frame is based on the 6U Supernova Bus of Pumpkin Inc. Electric propulsion will be used. An COTS engine that can provide the required Δv within the power and mass requirements is the Busek BIT-3³. The engine is also used for other CubeSat missions such as the Lunar Ice-Cube (Folta et al., 2016). With a wet weight of 3 kg

³http://www.busek.com/technologies_ion.htm

including 1.5 kg of propellant, the BIT-3 delivers a Δv of 3.2 km s^{-1} for a 13 kg CubeSat, when operated at 75 W power.

A Vacco cold-gas thruster and four star trackers complement the COTS attitude determination and control system. For power generation, the solar panel system MMA eHAWK with 96 W beginning-of-Life (BOL) has been chosen. The camera and a military rated JenOptic altimeter are mounted in the front next to the dipole antenna. Additionally 1U is occupied by housekeeping systems such as battery systems and an on-board computer. The green and yellow boxes represent the radar and communication system, respectively. The estimated weight of these systems leads to the total wet mass of the satellite, with 20 % margin of around 13.2 kg. The mass budget can be found in [Table 3](#).

Since the bistatic measurement process requires accurate timing, e.g., regarding radar pulse window synchronization, a chip-scale atomic clock (CSAC) will be needed on board in order to minimize all possible clocking differences between the two CubeSats ([DeNatale et al., 2008](#)). The synchronization accuracy provided natively by the CSAC will be around 100 ns^4 , that is, the travel-time corresponding to the maximal attainable radar accuracy (20 % of the range resolution, [Section 3.2](#)). The precision of the CSAC will allow a several hours' measurement time without re-synchronization, i.e., control pulse exchange.

4.2 Power requirement

In the science phase, the total peak power consumption will be about 50 W. The stepped frequency radar will require 40 W non-continuously in short pulses. The attitude control and housekeeping need together up to 10 W. During the cruise phase, the electric propulsion system requires most of the power. The desired Busek BIT-3 engine can be operated between 55 and 80 W. The efficiency of the engine will decrease along with the power consumption.

The MMA eHAWK is supplying solar arrays in the required scale. The HaWK 112-7058 delivers 96 W

⁴https://www.microsemi.com/document-portal/doc_view/133866-low-noise-csac-datasheet

BOL peak power⁵. The system consists, hereby, of two triple folded $2\text{U} \times 3\text{U}$ solar panels each mounted on one gimbaled root hinge. The power consumption estimates have been budgeted in [Table 3](#).

4.3 Antenna

Commercial systems using a motor have already proven the feasibility of a 3 m deployable antenna for Cubesats. In example Oxford Space ASTROTUBE BOOM has been validated in space, by unfolding to 1.5 m ([Reveles et al., 2017](#)). The Oxford system is available for length of up to 3 m and fits into 1U at a weight of 0.6 kg. Our half-length dipole antenna is projected to be build based on a metal strip design, which is widely utilized for antennas in space applications. A self-enrolling strip has been chosen as the design basis instead of a motor in order to reduce mass and volume of the system. The structure is slightly bent to be more stable and to function as a pre-stressed spring when rolled up. A thermal knife release the tapes, which unwinds entirely by rolling of the spacecraft. First unfolding tests have been successful. Currently, the stability during orbit maneuvers is under investigation.

4.4 Targets

In addition to the scientific and instrument requirements, the target needs to be reachable for a CubeSat. Based on a lunar transfer orbit, a study for an asteroid encountering mission with a 6U CubeSat has been performed by [Landis et al. \(2014\)](#). Landis argues that at least an initial Δv of 1.6 km s^{-1} into various asteroid orbits could be provided from the lunar transit insertion. Thus, the maximum possible total Δv will be 4.8 km s^{-1} , i.e., the sum of the Δv given by the thruster (3.2 km s^{-1}) and that of the lunar transit. As the detailed orbit analysis is still missing, we assume a margin of 0.8 km s^{-1} and limit our survey to asteroids with a Δv of maximally 4 km s^{-1} . Still, various asteroids fulfill this requirement. [Figure 5](#) shows targets⁶ on their closest approach that are reachable on various launch dates.

⁵<http://mmadesignllc.com/existing-hawk-configurations/>

⁶<https://cneos.jpl.nasa.gov/ca/>

Component	Specification	Availability	Mass (kg)	Power (W)
Bus	6U w. shielding	modif. COTS	2.0	
Solar panels	w. pointing	announced	1.0	96.0
Propulsion	Bit 3	COTS	3.0	56.0 to 80
Thruster	Cold gas, 50 Ns	COTS	0.6	0.0 to 10.0
Attitude control	2 mNm	COTS	1.0	0.5 to 2.0
Housekeeping	Incl. thermal	modif. COTS	1.0	2.0 to 7.0
Radar		TRL 3	1.0	40.0
Dipole antenna	2 × 3.75 m	TRL 2	0.4	
Atomic clock	Chip-Sized Atomic Clock	COTS	3.5 × 10 ⁻²	0.12
Nav. camera		modif. COTS	0.5	0.5 to 2.0
Laser altimeter		modif. COTS	0.05	0.01
Communication		TRL 2	1.5	10.0
Total			12.1 kg	
+ 20% Margin	w/o unmodif. COTS		13.2 kg	

Table 3: Mass and power budget for DISCUS. Note that the radar and electric propulsion are not running simultaneously. Power refers to nominal (non-peak) power. The radar power refers to the short stepped-frequency pulse sequences.

In our opinion, a good reference candidate for 2021 is the asteroid 65717 (1993 BX3)^{7 8} because of its close approach of 18.4 lunar distances (LD), relative Δv of around 3.6 km s⁻¹ in January 2021 and diameter between 180 and 410 m⁹. As the current discovery rate in the recent years has been around 1500 NEAs per year, more candidates could show up in the future. The selection of a mission target has to be revisited once when the final launch window has been fixed.

4.5 Radar measurement and mapping orbit

The two CubeSats will approach the targeted asteroid to a stable point between 5 km and 10 km altitude and perform their first radar measurements from a static position relative to the target. The mov-

⁷<https://ssd.jpl.nasa.gov/sbdb.cgi?sstr=65717>

⁸http://www.minorplanetcenter.net/db_search/show_object?utf8=%26amp;object_id=65717

⁹This size range is based on assumed geometric albedo p_V of $0.05 < p_V < 0.25$. There is an observation by Spitzer Space Telescope which gives, after radiometric analysis using techniques by Trilling et al. (2016), $D=91_{-15}^{+31}$ m and $p_V=0.72 \pm 0.33$ (<http://nearearthobjects.nau.edu/>). However, this albedo solution is unusually high as largest plausible albedos of NEOs are usually not much larger than 0.5 (Trilling et al., 2010). Therefore, we consider this result as a lower limit to the size of 65717 (1993 BX₃).

ing plane is supposed to avoid shadow phases, which would stress the thermal management and decrease the power generation. If the orbit of the spacecraft is polar, i.e., perpendicular to the spin of the asteroid, a single orbit will be sufficient to record a backscattering dataset for a nearly uniformly distributed set of measurement points enclosing the targeted NEA. We assume that a polar or nearly-polar polygonal orbit can be achieved with an orbiting direction that is perpendicular to the Solar System’s ecliptic plane, since most NEAs are known to have a retrograde spin (La Spina et al., 2004), i.e., the spin orientation is nearly normal to the ecliptic. The orbital movement of the spacecraft will be very slow. That is, the relative velocity between the asteroid’s surface and the spacecraft will be maximally a few meters per second and mainly determined by the spin period. Consequently, Doppler effects can be omitted. The exact duration of the measurements will depend on several parameters such as the asteroids spin period and orbiting distance. For example, a few weeks might be a sufficiently long period.

For positioning, we will apply the data provided by the radar and laser altimeter, star trackers, and the optical camera. The goal is to obtain an orientation accuracy of at least 3 degrees relative to the target asteroid’s surface, which has been suggested to be sufficient for tomography in (Takala et al., 2017c). The

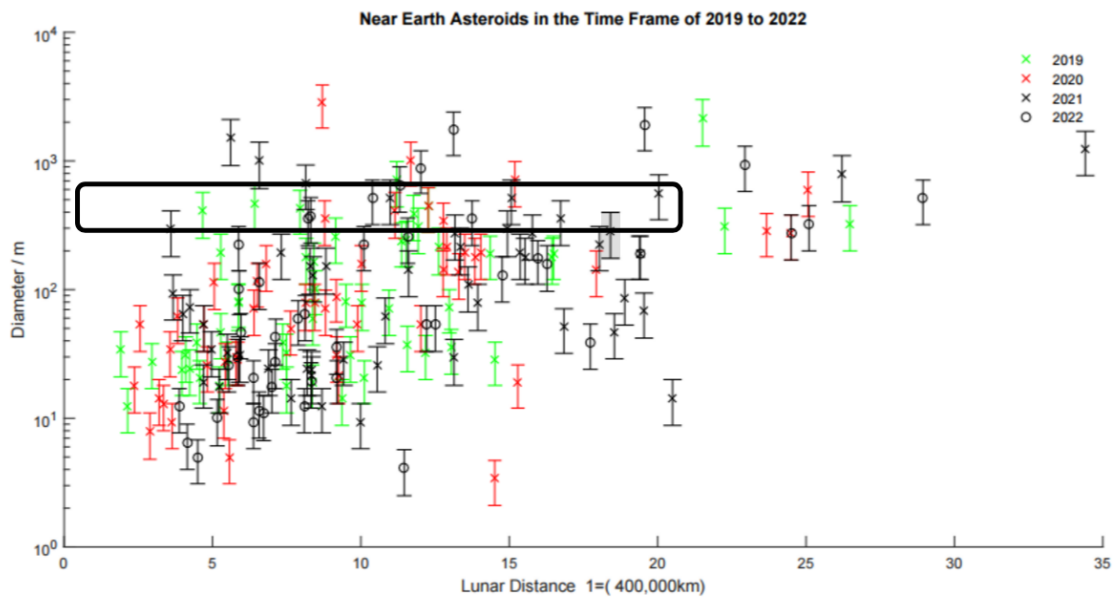


Figure 5: Potential targets in the 2010–2022 time frame. The black outlined box shows the most interesting target range with respect to the diameter and the distance of the closest approach. The gray box shows the asteroid 65717 (1993 B3) which is currently regarded as the most promising candidate with respect to the diameter (180 to 410 m), closest approach distance (18.4 lunar distances) and also Δv (3.6 km s^{-1}).

asteroid will be visible in the star trackers providing an accuracy around 0.01 degrees (Emright, 2010), e.g., with BST’s iADCS100. The distance to the asteroid can be obtained based on the altimeter data. Using the light-curve inversion, a preliminary estimate for the spin and shape model can be determined during the approach with an estimated couple of degrees accuracy for the spin (Durech et al., 2015). As suggested by our present analysis, the shape model can be refined up to an angular accuracy around one degree using the radar at the orbit (Section 3.2). A further refinement will be attempted via optical images.

In order to ensure that a robust tomographic reconstruction can be produced, we use a 1.5–2.0 spatial oversampling rate with respect to the Nyquist criterion (NC) which was suggested for a monochromatic (travel-time) measurement in (Pursiainen and Kaasalainen, 2015). This means recording the radar signal for 5000 to 20 000 measurement positions, when extrapolating the measurement positions to the close proximity of a targeted 260 to 600 m diameter NEA. The resulting estimated maximal amount of data recorded by a single satellite will be 250–1000 MB, respectively. Two identical CubeSats will be present in the mission. A perpendicular orbit will be used for both satellites. The measurement is bistatic, that is, one CubeSat both transmits and receives the signal and the other one serves as an additional receiver. In the measurements, the spacecraft will be placed within a constant angular distance from each other as seen from the asteroid (Takala et al., 2017a).

4.6 Data link

The essential prerequisite for the downlink is the ability to transfer the whole scientific dataset during the visibility to one ground-station on Earth. The size of the dataset is estimated to be about 12 to 13 Gibibit, coming from the radar (500 MiB), the camera (1025 MiB) and an altimeter (50 MiB). The size of the antenna is assumed to be 20 cm × 30 cm, the available transmit power is limited by the size of the spacecraft’s solar array. Our baseline strategy is to use the 35 m ESA Deep-Space Ground Sta-

tions capable to receive in the 31.8 to 32.3 GHz band. With a 3 W transmitter RF-power we expect that a data rate of about 520 Kibibit/s can be achieved using the DVB-S2 QPSK 2/3 operations mode. With this transfer rate a dataset of the estimated size can be transmitted to the Earth within less than 7 hours.

5 Discussion

In the DISCUS concept, a bistatic (two-spacecraft) low-frequency radar is carried by two CubeSats. The primary goal is to resolve the interior structure of a 260 to 600 m diameter, i.e., Itokawa-size (Abe et al., 2006), rubble pile asteroid. Based on this study, the most promising target candidate is currently 65717 (1993 BX3), a potentially hazardous object, which will make its next close Earth approach in 2021 at a Δv of 3.6 km s⁻¹ with the closest point being at 18.4 lunar distances from the Earth. More candidates will probably be detected in the near future, and the final target asteroid can only be selected when a launch opportunity has been found.

Akin to airborne GPR, the radar design is based on the stepped-frequency measurement technique coupled with a linear dipole antenna (Fu et al., 2014). We aim to use a low 20–50 MHz signal frequency in order to maximize the signal penetration depth (Francke and Utsi, 2009; Leucci, 2008; Kofman, 2012) and, thereby, to obtain a global data coverage for the interior part. The main mission objective will be achieved, if the internal macroporosity structures can be detected and mapped. We expect that full or close to full penetration will be achieved, since the level of the signal attenuation in the porous minerals of planetary subsurfaces in the planned low frequency range is known to be low (Kofman, 2012), e.g., 10 to 30 dB km⁻¹ for basalt. Also the outcome of CONSERT shows that signal penetration through an small Solar System body of two times the targeted size range can be achieved (Kofman et al., 2015). Moreover, the estimated data transfer capacity (Section 4.6) allows recording the signal for a sufficiently dense distribution of points within targeted size range (Section 4.5).

Our recent simulation study (Takala et al., 2017a)

suggests that the tomographic reconstruction of the interior details, such as voids, will be feasible. Based on the results, we expect that the interior can be reconstructed, if the total noise including both measurement and modeling errors is at least 5 to 10 dB below the signal amplitude. This was observed to be the case in CONSERT (comet 67P/Churyumov-Gerasimenko), where the secondary signal peaks were mainly 20 dB below the main peak (Kofman et al., 2015). Due to the relatively high electric permittivity of the asteroid materials we expect a somewhat higher error level for an asteroid. The results of (Takala et al., 2017a), furthermore, suggest that also limited-angle measurements following from a non-perpendicular (non-polar) orbit will allow obtaining a reconstruction. That is, also NEAs with an exceptional (non-retrograde) spin (La Spina et al., 2004) are potential targets for tomographic reconstruction. In the numerical simulations, we have assumed a 25 dB km^{-1} signal attenuation level. In practice, the scattering caused by the macroporosity can lead to some additional attenuation.

The targeted 2 MHz total bandwidth for the stepped-frequency measurements would give the resolution of at least 20 to 40 m inside the target asteroid (Daniels, 2005), if its relative permittivity is 3 to 12 (e.g. solid and pulverized rocks and silica). This would mean the distinguishability of the details around the size 1/20–1/10 with respect to the asteroid diameter providing an unforeseen reconstruction accuracy for the deep interior structure. Consequently, the current design should be sufficient for the main goal of detecting major variances in the volumetric relative electric permittivity structure. For comparison, the initial maximal resolution estimates for CONSERT and *Deep Interior* were 16 and 20 m, respectively (Kofman et al., 2007; Asphaug et al., 2003). In CONSERT, the carrier frequency and bandwidth of the signal were 90 and 8 MHz, respectively.

We consider the 2 MHz bandwidth advantageous from both computational and measurement viewpoints, as we currently can invert a full set of data for the targeted asteroid size (Takala et al., 2017a) and sufficient measurement accuracy seems achievable. A wider bandwidth would, however, allow distinguish-

ing smaller details. Techniques to increase the bandwidth can, in principle, include adding transmission channels and modifying the antenna folding, loading and increasing the width (Fu et al., 2014; Poggio and Mayes, 1971; Balanis, 2012; Alexander et al., 2002). Nevertheless, each of these adjustments would increase the complexity, total weight and power consumption of the system and, therefore, those are not suggested for the initial design. Our initial hardware design relies on optimizing the weight and size of the spacecraft in order to minimize the mission costs. Therefore, the 6U frame is used as the reference design. Based on this study, the 75 W Busek BIT-3 thruster will be able to provide the 6U CubeSat a Δv of 3.2 km s^{-1} which together with an initial Δv obtained from a lunar transfer orbit (Landis et al., 2014) will result in a total Δv of approximately 4 km s^{-1} . This would be enough to reach, e.g., the asteroid 65717 (1993 BX3) in 2021. Depending on the eccentricity of the transfer orbit the targeted 75 W cannot be achieved for the entire transfer. Yet, we expect that including the initial Δv , the required power for the thruster will have enough margins to compensate these phases. In the current design the total Δv is limited mainly by the power provided by the solar cells, as they degrade over time and produce less power at sun distances beyond 1 AU. The number of reachable targets would increase if solar cells with 120 W are used, as the potential of the propulsion system could then be used to the full extend. With currently available solar panels this would be the mass by 0.8 kg.

A larger 12U size can also be considered, even if all components would fit in the 6U bus and other authors have described the envelope as feasible (Frick et al., 2014; Staehle et al., 2013). Namely, the margins are small and could be eaten up by any insertion in the radar, communication system or thermal management. Nevertheless, a 12U bus would lead to a higher total weight and, consequently, require a much larger orbit control system. As the power would not necessarily scale with size, a completely different propulsion system would be needed. One possibility to overcome the possible issues would be a piggy-bag ride to an asteroid. This would reduce the need of Δv and communication capability and might lead to

an extra 3/2 U of scientific payload, for instance, a more advanced camera system.

The proposed self-rolled half-wavelength dipole antenna design is beneficial with respect to the mass and volume. We emphasize that the present antenna specifications have been designed for Itokawa-size bodies for which a well-penetrating signal frequency is necessary. Nevertheless, the radar and the spacecraft can also operate with higher frequencies and shorter antenna lengths, which might be preferable for smaller bodies or shallower subsurface structures. In any case COTS solutions at slightly higher weight are available.

We consider that the goal to fit the radar in a 1U (1000 cm³) space is feasible based on RST's earlier experience of the 900 cm³ HOPE radar design (RST Radar Systemtechnik AG, 2001). The next development stage aim to build a 20 MHz radar demonstrator to validate the proposed instrumentation in an on-ground test. RST GmbH has previous experience of such an experiment from ESA's project PIRA (Braun et al., 1997) in which a stepped-frequency radar equipped with a sub 10 MHz orbiter antenna system was successfully tested under motion. An ongoing work is to transfer the existing radar design to a below 100 MHz frequency band.

Compared to more frequently used microwave CubeSat radars, for example, Raincube's 4U and 10 W Ka-band radar (Peral et al., 2017), the planned low-frequency band allows a more simple design. Attaining a considerably better synchronization than what is natively provided by the CSAC, e.g., due to a wider bandwidth, might necessitate extra arrangements. For example, in the recent microwave-range interferometry measurements of the TandDEM-X mission, obtaining a picosecond-level synchronization required relative phase referencing via six dedicated synchronization horn antennas in each spacecraft (Krieger et al., 2007).

Future work will include construction of a demonstrator prototype to validate the radar. Numerical simulations concerning the stepped-frequency measurement technique, shape modeling, and also orbit calculations around the asteroid will be performed. We will also examine the capability of the planned instrumentation, e.g., regarding flyby measurements,

to reconstruct the interior of a comet and also in mapping of the recently discovered Moon caves. Several details will need to be refined in the final design stage.

6 Conclusion

DISCUS - The Deep Interior Scanning CubeSat mission is designed with the aim to characterize the interior structure of rubble pile asteroids. Computed radar tomography and a bistatic configuration of two identical CubeSats will be used to reconstruct internal electric permittivity heterogeneities. While deep-space missions for CubeSat sized spacecraft are still a challenge from an engineering point of view, we found that our radar is compatible with the limitations of a CubeSat mission to a near-Earth asteroid. The baseline design of the DISCUS spacecraft provides a Δv of 3.2 km s⁻¹. A launch to a lunar transfer orbit provides an additional Δv so that asteroids with a Δv of approximately 4 km s⁻¹ are reachable. The most prominent target candidate among the currently known NEAs is 65 717 (1993 BX3).

The main scientific result that could be accomplished with DISCUS mission is mapping the distribution of porosity within a rubble pile asteroid. This would be on the one hand of great value to formation models of the Solar System, but also of great importance to deflection scenarios for potentially hazardous asteroids imposing an impact threat to earth. Additionally, crucial knowledge of the internal permittivity structures and, thereby, also the mineral content of the asteroids would be obtained.

Acknowledgments

MT and SP were supported by the Academy of Finland Key Project 305055 and AoF Centre of Excellence in Inverse Problems.

PB, JD and EV were supported by the Max Planck Institute for Solar System research.

References

- Abe, S., Mukai, T., Hirata, N., Barnouin-Jha, O. S., Cheng, A. F., Demura, H., Gaskell, R. W., Hashimoto, T., Hiraoka, K., Honda, T., Kubota, T., Matsuoka, M., Mizuno, T., Nakamura, R., Scheeres, D. J., Yoshikawa, M., 2006. Mass and Local Topography Measurements of Itokawa by Hayabusa. *Science* 312 (5778), 1344–1347.
- Alexander, M., Salter, M., Loader, B., Knight, D., 2002. Broadband calculable dipole reference antennas. *IEEE Transactions on electromagnetic compatibility* 44 (1), 45–58.
- Asmar, S., Matousek, S., 2014. Mars Cube one (MarCO): The first planetary CubeSat mission. In: *Proceedings of the Mars CubeSat/NanoSat Workshop*, Pasadena, California, November. Vol. 20. p. 21.
- Asphaug, E., Belton, M., Cangahuala, A., Keith, L., Klaasen, K., McFadden, L., Neumann, G., Ostro, S., Reinert, R., Safaeinili, A., et al., 2003. Exploring asteroid interiors: The Deep Interior mission concept. In: *Lunar and Planetary Science Conference*. Vol. 34.
- Balanis, C., 2012. *Antenna Theory: Analysis and Design*. Wiley.
- Barnouin-Jha, O. S., Cheng, A. F., Mukai, T., Abe, S., Hirata, N., Nakamura, R., Gaskell, R. W., Saito, J., Clark, B. E., 2008. Small-scale topography of 25143 Itokawa from the Hayabusa laser altimeter. *Icarus* 198 (1), 108 – 124.
- Braun, H., Lentz, H., Woode, A., 1997. A Planetary Into-the-Ground Radar and Altimeter (PIRA). In: *Applied Geologic Remote Sensing - International Conference*. Vol. 1. pp. I–498.
- Carry, B., 2012. Density of asteroids. *Planetary and Space Science* 73 (1), 98–118.
- Clark, P., Malphrus, B., Brown, K., Reuter, D., MacDowall, R., Folta, D., Mandell, A., Hurford, T., Brambora, C., Patel, D., et al., 2016. Lunar Ice Cube Mission: Determining Lunar Water Dynamics with a First Generation Deep Space CubeSat. *Science* 330, 463–468.
- Daniels, D. J., 2005. *Ground penetrating radar*. Wiley Online Library.
- Deller, J. F., 2017. *Hyper-Velocity Impacts on Rubble Pile Asteroids*. Ph.D. thesis, School of Physical Sciences University of Kent Canterbury U.K. and International Max Planck Research School for Solar System Science Göttingen Germany.
- DeNatale, J., Borwick, R., Tsai, C., Stupar, P., Lin, Y., Newgard, R., Berquist, R., Zhu, M., 2008. Compact, low-power chip-scale atomic clock. In: *Position, Location and Navigation Symposium, 2008 IEEE/ION*. IEEE, pp. 67–70.
- Ďurech, J., Carry, B., Delbo, M., Kaasalainen, M., Viikinkoski, M., 2015. Asteroid models from multiple data sources. *Asteroids IV*, 183.
- Eisenburger, D., Lentz, H., Jenett, M., 2008. Helicopter-borne GPR systems: A way from ice thickness measurements to geological applications. In: *Ultra-Wideband, 2008. ICUWB 2008. IEEE International Conference on*. Vol. 3. IEEE, pp. 161–165.
- Enright, J., 2010. Moon-tracking modes for star trackers. *Journal of guidance, control, and dynamics* 33 (1), 171–185.
- Erst, S. J., 1984. *Receiving systems design*. Artech House on Demand, Dedham, Massachusetts.
- Farinella, P., Paolicchi, P., Zappalá, V., Dec. 1982. The asteroids as outcomes of catastrophic collisions. *Icarus* 52, 409–433.
- Folta, D. C., Bosanac, N., Cox, A., Howell, K. C., 2016. The Lunar IceCube mission design: construction of feasible transfer trajectories with a constrained departure. *NASA Technical Reports Server (AAS 16-285)*. URL <https://ntrs.nasa.gov/archive/nasa/casi.ntrs.nasa.gov/20170001470.pdf>

- Francke, J., Utsi, V., 2009. Advances in long-range GPR systems and their applications to mineral exploration, geotechnical and static correction problems. *First Break* 27 (7).
- Frick, A., Castillo-Rogez, J., Johnson, L., Dervan, J., 2014. NEA Scout: A CubeSat Architecture for Near Earth Asteroid (NEA) Exploration. In: *Proceedings of Interplanetary Small Satellite Conference (ISSC)*.
- Fu, L., Liu, S., Liu, L., Lei, L., 2014. Development of an airborne ground penetrating radar system: antenna design, laboratory experiment, and numerical simulation. *IEEE Journal of selected topics in applied Earth observations and remote sensing* 7 (3), 761–766.
- Gundelach, V., Blindow, N., Buschmann, U., Salat, C., Krellmann, Y., 2010. Exploration of geological structures with GPR from helicopter and on the ground in the Letzlinger Heide (Germany). In: *Ground Penetrating Radar (GPR), 2010 13th International Conference on*. IEEE, pp. 1–6.
- Herique, A., Ciarletti, V., 2016. A Direct Observation of the Asteroids Structure from Deep Interior to Regolith: Two Radars on the AIM Mission. In: *47th Lunar and Planetary Science Conference*. p. 2096.
- Hodges, R. E., Chahat, N. E., Hoppe, D. J., Vaccione, J. D., 2016. The Mars Cube One deployable high gain antenna. In: *Antennas and Propagation (APSURSI), 2016 IEEE International Symposium on*. IEEE, pp. 1533–1534.
- Imken, T., Castillo-Rogez, J., He, Y., Baker, J., Marinan, A., 2017. Cubesat flight system development for enabling deep space science. In: *Aerospace Conference, 2017 IEEE*. IEEE, pp. 1–14.
- Ishiguro, M., Nakamura, R., Tholen, D. J., Hirata, N., Demura, H., Nemoto, E., Nakamura, A. M., Higuchi, Y., Sogame, A., Yamamoto, A., Kitazato, K., Yokota, Y., Kubota, T., Hashimoto, T., Saito, J., Jun. 2010. The Hayabusa Spacecraft Asteroid Multi-band Imaging Camera (AMICA). *Icarus* 207, 714–731.
- Jol, H. M., 2008. *Ground Penetrating Radar Theory and Applications*. Elsevier Science.
- Kofman, W., 2012. Radar techniques to study sub-surfaces and interiors of the solar system objects. In: *Microwave Radar and Wireless Communications (MIKON), 2012 19th International Conference on*. Vol. 2. IEEE, pp. 409–412.
- Kofman, W., Herique, A., Barbin, Y., Barriot, J.-P., Ciarletti, V., Clifford, S., Edenhofer, P., Elachi, C., Eyraud, C., Goutail, J.-P., Heggy, E., Jorda, L., Lasue, J., Lvasseur-Regourd, A.-C., Nielsen, E., Pasquero, P., Preusker, F., Puget, P., Plettemeier, D., Rogez, Y., Sierks, H., Statz, C., Svedhem, H., Williams, I., Zine, S., Van Zyl, J., 2015. Properties of the 67P/Churyumov-Gerasimenko interior revealed by CONSERT radar. *Science* 349 (6247).
- Kofman, W., Herique, A., Goutail, J.-P., Hagfors, T., Williams, I. P., Nielsen, E., Barriot, J.-P., Barbin, Y., Elachi, C., Edenhofer, P., Lvasseur-Regourd, A.-C., Plettemeier, D., Picardi, G., Seu, R., Svedhem, V., 2007. The comet nucleus sounding experiment by radiowave transmission (CONSERT): A short description of the instrument and of the commissioning stages. *Space Science Reviews* 128 (1–4), 413–432.
- Kraus, J., 1966. *Radio astronomy*. McGraw-Hill.
- Krieger, G., Moreira, A., Fiedler, H., Hajnsek, I., Werner, M., Younis, M., Zink, M., 2007. TanDEM-X: A satellite formation for high-resolution SAR interferometry. *IEEE Transactions on Geoscience and Remote Sensing* 45 (11), 3317–3341.
- Kwiatkowski, T., Jan. 2010. Photometric survey of the very small near-Earth asteroids with the SALT telescope. *Astronomy and Astrophysics* 509, A95.
- La Spina, A., Paolicchi, P., Kryszczyńska, A., Pravec, P., 2004. Retrograde spins of near-Earth asteroids from the Yarkovsky effect. *Nature* 428 (6981), 400.
- Lacomme, P., 2001. *Air and Spaceborne Radar Systems: An Introduction*. Electronics & Electrical. William Andrew.

- Landis, G. A., Oleson, S. R., McGuire, M. L., Burke, L. M., Martini, M. C., Fittje, J. E., Packard, T. W., 2014. A cubesat asteroid mission: Propulsion trade-offs. In: 50th AIAA/ASME/SAE/ASEE Joint Propulsion Conference. AIAA Propulsion and Energy Forum. American Institute of Aeronautics and Astronautics.
- Lentz, H., Braun, H., 2000. GINGER II An upgrade of the technology demonstrator of the guidance and into the ground exploration radar GINGER. *Advanced Space Technologies for Robotics and Automation (ASTRA 2000)*, ESTEC, Noordwijk, Holland, paper (3.5).
- Leucci, G., 2008. Ground Penetrating Radar: The Electromagnetic Signal Attenuation and Maximum Penetration Depth. *Scholarly Research Exchange* 2008.
- Manasse, R., 1960. Summary of maximum theoretical accuracy of radar measurements. Tech. rep., MITRE CORP BEDFORD MA.
- Michel, P., DeMeo, F., Bottke, W., 2015. Asteroids IV. *Space Science Series*. University of Arizona Press.
- Michel, P., Kueppers, M., Carnelli, I., Galvez, A., Mellab, K., Cheng, A., 2016. Asteroid Impact Mission (AIM): The European component of the AIDA space project. In: *Lunar and Planetary Science Conference*. Vol. 47. p. 1204.
- Michel, P. P., Benz, W. W., Tanga, P., Richardson, D. C., Nov. 2001. Collisions and Gravitational Reaccumulation: Forming Asteroid Families and Satellites. *Science* 294 (5547), 1696–1700.
- Michel, P. P., Benz, W. W., Tanga, P., Richardson, D. C., Nov. 2002. Formation of Asteroid Families by Catastrophic Disruption: Simulations with Fragmentation and Gravitational Reaccumulation. *Icarus* 160 (1), 10–23.
- Michikami, T., Nakamura, A. M., Hirata, N., Gaskell, R. W., Nakamura, R., Honda, T., Honda, C., Hiraoka, K., Saito, J., Demura, H., Ishiguro, M., Miyamoto, H., 2008. Size-frequency statistics of boulders on global surface of asteroid 25143 Itokawa. In: *Earth Planets and Space*. Fukushima Natl Coll Technol, Iwaki, Fukushima 9708034, Japan, pp. 13–20.
- Nakamura, T., Nakamura, A. M., Saito, J., Sasaki, S., Nakamura, R., Demura, H., Akiyama, H., Tholen, D., et al., 2001. Multi-band imaging camera and its sciences for the Japanese Near-Earth asteroid mission MUSES-C. *Earth, Planets and Space* 53 (11), 1047–1063.
- NASA Mission Design Division, 2015. Small spacecraft technology state of the art. https://www.nasa.gov/sites/default/files/atoms/files/small_spacecraft_technology_state_of_the_art_2015_tagged.pdf, accessed: 2017-10-05.
- Peral, E., Statham, S., Taneli, S., Imken, T., Williams, A., Price, D., Sauder, J., Chahat, N., 2017. RainCube, a Ka-band Precipitation Radar in a 6U CubeSat. In: *31st Annual AIAA/USU Conference on Small Satellites*.
- Poggio, A., Mayes, P., 1971. Bandwidth extension for dipole antennas by conjugate reactance loading. *IEEE Transactions on Antennas and Propagation* 19 (4), 544–547.
- Pravec, P., Harris, A. W., Nov. 2000. Fast and Slow Rotation of Asteroids. *Icarus* 148, 12–20.
- Pravec, P., Harris, A. W., Michalowski, T., 2002. Asteroid rotations. *Asteroids III* 113.
- Pursiainen, S., Kaasalainen, M., 2015. Electromagnetic 3D subsurface imaging with source sparsity for a synthetic object. *Inverse Problems* 31 (12), 125004.
- Putz, P., Woode, A., Braun, H.-M., 1997. Ginger - a radar instrument for planetary rover applications. *Preparing for the Future* 7 (2), 14.
- Rahmat-Samii, Y., Manohar, V., Kovitz, J. M., 2017. For satellites, think small, dream big: A review of recent antenna developments for cubesats. *IEEE Antennas and Propagation Magazine* 59 (2), 22–30.

- Reveles, J., Lawton, M., Fraux, V., Gurusamy, V., Parry, V., 2017. In-orbit performance of astrotube: Alsat nano’s low mass deployable composite boom payload.
- Richardson, D. C., Leinhardt, Z. M., Melosh, H. J., Bottke, W. F., Asphaug, E., Oct. 2002. Gravitational Aggregates: Evidence and Evolution. In: Bottke, W. F., Cellino, A., Paolicchi, P., Binzel, R. P. (Eds.), *Asteroids III*. University of Arizona Press, pp. 501–515.
- Rozitis, B., MacLennan, E., Emery, J. P., Aug. 2014. Cohesive forces prevent the rotational breakup of rubble-pile asteroid (29075) 1950 DA. *Nature* 512 (7513), 174–176.
- RST Radar Systemtechnik AG, 2001. HOPE (Handheld Operated Demining System). http://www.rst-group.biz/index.php?id=113&no_cache=1, accessed: 2017-10-05.
- Rutishauser, A., Maurer, H., Bauder, A., 2016. Helicopter-borne ground-penetrating radar investigations on temperate alpine glaciers: A comparison of different systems and their abilities for bedrock mapping. *Geophysics* 81 (1), WA119–WA129.
- Safaenili, A., Gulkis, S., Hofstadter, M. D., Jordan, R. L., Dec. 2002. Probing the interior of asteroids and comets using radio reflection tomography. *Meteoritics and Planetary Science* 37, 1953–1963.
- Saito, J., Miyamoto, H., Nakamura, R., Ishiguro, M., Michikami, T., Nakamura, A. M., Demura, H., Sasaki, S., Hirata, N., Honda, C., Yamamoto, A., Yokota, Y., Fuse, T., Yoshida, F., Tholen, D. J., Gaskell, R. W., Hashimoto, T., Kubota, T., Higuchi, Y., Nakamura, T., Smith, P., Hiraoka, K., Honda, T., Kobayashi, S., Furuya, M., Matsumoto, N., Nemoto, E., Yukishita, A., Kitazato, K., Dermawan, B., Sogame, A., Terazono, J., Shinohara, C., Akiyama, H., 2006. Detailed Images of Asteroid 25143 Itokawa from Hayabusa. *Science* 312 (5778), 1341–1344.
- Sánchez, P., Scheeres, D. J., Apr. 2012. DEM simulation of rotation-induced reshaping and disruption of rubble-pile asteroids. *Icarus* 218 (2), 876–894.
- Snodgrass, C., Jones, G., Boehnhardt, H., Gibbings, A., Homeister, M., Andre, N., Beck, P., Bentley, M., Bertini, I., Bowles, N., Capria, M., Carr, C., Ceriotti, M., Coates, A., Corte, V. D., Hanna, K. D., Fitzsimmons, A., Gutierrez, P., Hainaut, O., Herique, A., Hilchenbach, M., Hsieh, H., Jehin, E., Karatekin, O., Kofman, W., Lara, L., Laudan, K., Licandro, J., Lowry, S., Marzari, F., Masters, A., Meech, K., Moreno, F., Morse, A., Orosei, R., Pack, A., Plettemeier, D., Prialnik, D., Rotundi, A., Rubin, M., Sanchez, J., Sheridan, S., Trieloff, M., Winterboer, A., 2017. The Castalia mission to Main Belt Comet 133P/Elst-Pizarro. *Advances in Space Research*.
- Staehle, R., Blaney, D., Hemmati, H., Lo, M., Mouroulis, P., Pingree, P., Wilson, T., Puig-Suari, J., Williams, A., Betts, B., et al., 2013. Interplanetary CubeSats: opening the solar system to a broad community at lower cost. *Journal of small satellites* 2 (1), 161–186.
- Takala, M., Bambach, P., Deller, J., Vilenus, E., Wittig, M., Lentz, H., Braun, H. M., Kaasalainen, M., Pursiainen, S., 2017a. A far-field inversion approach for the deep interior scanning cubesat. arXiv preprint arXiv:1709.04309.
- Takala, M., Hämäläinen, T. D., Pursiainen, S., 2017b. The Effect of Hardware-Computed Travel Time on Localization Accuracy in the Inversion of Experimental (Acoustic) Waveform Data. *IEEE Transactions on Computational Imaging* 3 (2), 344–354.
- Takala, M., Us, D., Pursiainen, S., 2017c. Multigrid-based inversion for volumetric radar imaging with asteroid interior reconstruction as a potential application. arXiv preprint arXiv:1707.04605.
- Thirouin, A., Moskovitz, N., Binzel, R. P., Christensen, E., DeMeo, F. E., Person, M. J., Polishook, D., Thomas, C. A., Trilling, D., Willman, M., Hinkle, M., Burt, B., Avner, D., Aceituno, F. J., Nov. 2016. The mission accessible Near-Earth Objects survey (MANOS): First photometric results. *The Astronomical Journal* 152 (6), 163.

- Tricarico, P., Mar. 2017. The near-Earth asteroid population from two decades of observations. *Icarus* 284, 416–423.
- Trilling, D. E., Mommert, M., Hora, J., Chesley, S., Emery, J., Fazio, G., Harris, A., Mueller, M., Smith, H., Dec. 2016. NEOSurvey 1: Initial Results from the Warm Spitzer Exploration Science Survey of Near-Earth Object Properties. *Astronomical Journal* 152, 172.
- Trilling, D. E., Mueller, M., Hora, J. L., Harris, A. W., Bhattacharya, B., Bottke, W. F., Chesley, S., Delbo, M., Emery, J. P., Fazio, G., Mainzer, A., Penprase, B., Smith, H. A., Spahr, T. B., Stansberry, J. A., Thomas, C. A., Sep. 2010. Explore-NEOs. I. Description and First Results from the Warm Spitzer Near-Earth Object Survey. *Astronomical Journal* 140, 770–784.
- Walker, R., Koschny, D., Bramati, C., Carnelli, I., ESA, C. S. T., 2017. Miniaturised Asteroid Remote Geophysical Observer (M-ARGO): a stand-alone deep space CubeSat system for low-cost science and exploration missions. In: *iCubeSat 7 abstracts*.
- Walsh, K. J., Richardson, D. C., Michel, P. P., Jul. 2008. Rotational breakup as the origin of small binary asteroids. *Nature* 454 (7201), 188–191.